Banded structures in electron pitch angle diffusion coefficients from resonant wave-particle interactions

A. K. Tripathi, R. P. Singhal, G. V. Khazanov, and L. A. Avanov

Citation: Physics of Plasmas **23**, 042101 (2016); doi: 10.1063/1.4944920
View online: http://dx.doi.org/10.1063/1.4944920
View Table of Contents: http://scitation.aip.org/content/aip/journal/pop/23/4?ver=pdfcov
Published by the AIP Publishing

Banded structures in electron pitch angle diffusion coefficients from resonant wave-particle interactions

A. K. Tripathi,[1,a)] R. P. Singhal,[1,b)] G. V. Khazanov,[2,c)] and L. A. Avanov[2,3,d)]
[1]*Department of Physics, Indian Institute of Technology (Banaras Hindu University), Varanasi, Uttar Pradesh, India*
[2]*NASA Goddard Space Flight Center, Greenbelt, Maryland 20771, USA*
[3]*Department of Astronomy, University of Maryland, College Park, Maryland 20742, USA*

(Received 24 October 2015; accepted 15 March 2016; published online 4 April 2016)

Electron pitch angle ($D_{\alpha\alpha}$) and momentum (D_{pp}) diffusion coefficients have been calculated due to resonant interactions with electrostatic electron cyclotron harmonic (ECH) and whistler mode chorus waves. Calculations have been performed at two spatial locations L = 4.6 and 6.8 for electron energies ≤10 keV. Landau (n = 0) resonance and cyclotron harmonic resonances n = ±1, ±2, … ±5 have been included in the calculations. It is found that diffusion coefficient versus pitch angle (α) profiles show large dips and oscillations or banded structures. The structures are more pronounced for ECH and lower band chorus (LBC) and particularly at location 4.6. Calculations of diffusion coefficients have also been performed for individual resonances. It is noticed that the main contribution of ECH waves in pitch angle diffusion coefficient is due to resonances n = +1 and n = +2. A major contribution to momentum diffusion coefficients appears from n = +2. However, the banded structures in $D_{\alpha\alpha}$ and D_{pp} coefficients appear only in the profile of diffusion coefficients for n = +2. The contribution of other resonances to diffusion coefficients is found to be, in general, quite small or even negligible. For LBC and upper band chorus waves, the banded structures appear only in Landau resonance. The D_{pp} diffusion coefficient for ECH waves is one to two orders smaller than $D_{\alpha\alpha}$ coefficients. For chorus waves, D_{pp} coefficients are about an order of magnitude smaller than $D_{\alpha\alpha}$ coefficients for the case n ≠ 0. In case of Landau resonance, the values of D_{pp} coefficient are generally larger than the values of $D_{\alpha\alpha}$ coefficients particularly at lower energies. As an aid to the interpretation of results, we have also determined the resonant frequencies. For ECH waves, resonant frequencies have been estimated for wave normal angle 89° and harmonic resonances n = +1, +2, and +3, whereas for whistler mode waves, the frequencies have been calculated for angle 10° and Landau resonance. Further, in ECH waves, the banded structures appear for electron energies ≥1 keV, and for whistler mode chorus waves, structures appear for energies >2 keV at L = 4.6 and above 200 eV for L = 6.8. The results obtained in the present work will be helpful in the study of diffusion curves and will have important consequences for diffuse aurora and pancake distributions.
 [http://dx.doi.org/10.1063/1.4944920]

I. INTRODUCTION

Pitch-angle diffusion of plasma-sheet electrons into the atmospheric loss-cone leads to an electron precipitation producing diffuse aurora.[1] Scattering of electrons is predominantly controlled by resonant wave-particle interactions. Two important plasma wave modes that are mainly responsible for these interactions are whistler mode chorus waves and electrostatic electron cyclotron harmonic (ECH) waves. Whistler mode chorus waves are electromagnetic waves that propagate in the right-handed polarized whistler mode with frequency below electron gyro-frequency (f_{ce}). These waves typically occur in two frequency bands: 0.1–0.5 f_{ce} and 0.5–0.8 f_{ce} called lower band chorus (LBC) and upper band chorus (UBC), respectively, with an emission gap at 0.5 f_{ce}.[2–5] They propagate in general parallel or quasi-parallel to the ambient magnetic field. Some of earliest observations found that the wave normal angles (θ) for LBC were field aligned within a cone of angles less than 20° near the equator and became more oblique with increasing latitude.[6] Several case events revealed large angles $\theta = 30°$–45°. For UBC, the angle θ was typically up to about 50°. More recent studies[7] show that the highest probability of occurrence is for wave normal angles less than 42°. Nightside chorus also tends to propagate with wave normal angles smaller than those for dayside chorus.

ECH waves are electrostatic emissions observed in bands between the harmonics of the electron gyro-frequency and are sometimes called "n + 1/2" waves since the emissions tend to appear close to the odd integral half harmonics of the f_{ce}. These waves propagate at very large angles with respect to the ambient magnetic field.[8] Pitch-angle diffusion by ECH waves has been studied in several works.[9–15] Pitch-angle diffusion by whistler mode chorus waves has also been studied extensively.[13,16–20] In a very recent study,[21] calculations of pitch-angle diffusion coefficients have been performed due to both ECH and whistler mode chorus waves in the course of studies related to the electron distribution function formation in the

[a)]Electronic mail: aktrip2001@yahoo.co.in
[b)]Electronic mail: rpsiitbhu@yahoo.com
[c)]Author to whom correspondence should be addressed. Electronic mail: George.V.Khazanov@nasa.gov
[d)]Electronic mail: levon.a.avanov@nasa.gov

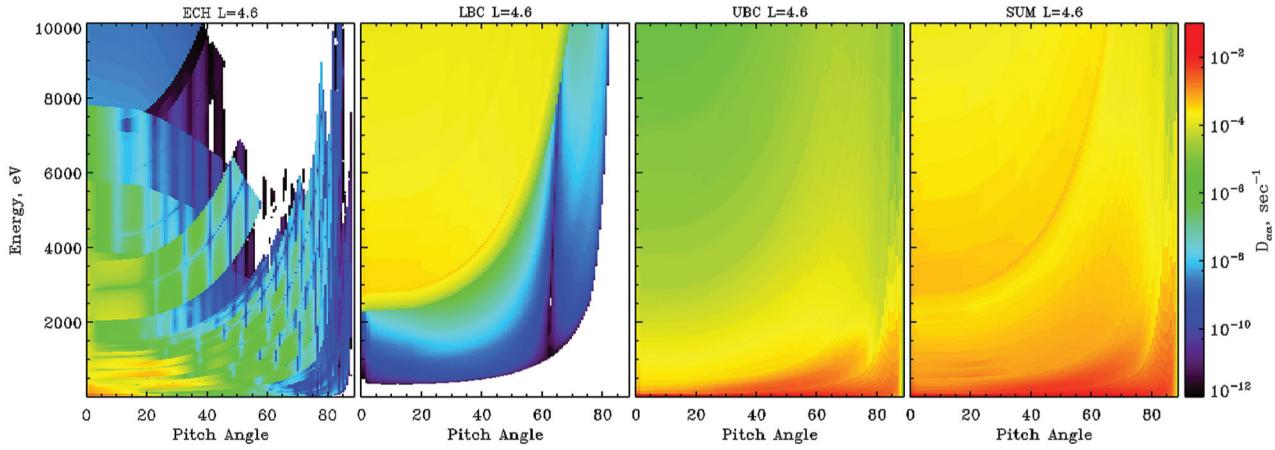

FIG. 1. Pitch angle diffusion coefficients ($D_{\alpha\alpha}$) versus pitch angle (α) corresponding to energies from 1 eV to 10 keV for ECH (first column), LBC (second column), and UBC (third column), as well as their SUM (last column) at L = 4.6.

L-shell corresponding to the diffuse aurora region. Local diffusion coefficients have been calculated for electron energies between 1 eV and 10 keV at energy grid spacing of 1 eV and at 135 pitch-angles between 0° and 90°. Calculations have been performed at two spatial locations, L = 4.6 and 6.8. These are presented in Figs. 1 and 2. An important finding of the diffusion coefficients calculations is the appearance of structures, particularly large dips, oscillations, and gaps in profile of diffusion coefficients versus pitch angle (PA). These so called banded structures are more pronounced for ECH and LBC waves at location 4.6 as may be noted from Fig. 1. Furthermore, to complete the present study, we have also calculated and analyzed the momentum and energy diffusion coefficients for ECH and whistler mode waves. Although much work has already been done on this topic[22–24] involving chorus waves at relativistic electron energies in the outer radiation belt, we present a comparative analysis of structures in pitch-angle and momentum diffusion coefficients at electron energies $\leq$10 keV. The objective of the present study is to investigate the origin of banded structures in diffusion coefficients due to ECH and whistler mode waves. These studies would help to draw significant conclusions on the effect that these waves have on electrons.

The paper is organized as follows: Expressions for diffusion coefficients for ECH and whistler mode waves are given in Section II. Section III presents the details for calculating resonant frequencies due to resonant wave-particle interactions. All results are discussed in Section IV, and Section V presents conclusions of the present study.

II. DIFFUSION COEFFICIENTS

A. ECH waves

The pitch-angle diffusion coefficients for electrostatic ECH waves, in units of per second, are given as[9]

$$D_{\alpha\alpha} = \sum_{n=-\infty}^{\infty} \int k_\perp dk_\perp \left[\psi_{n,k} \left(\frac{(n\,\Omega_e/\omega_k) - \sin^2\alpha}{\sin\alpha\cos\alpha} \right)^2 \right]_{k_\parallel = k_{\parallel res}}, \quad (1)$$

where

$$\psi_{n,k} = \frac{e^2}{4\,\pi\,m_e^2} \frac{|E_k|^2}{V} \left(\frac{\omega_k}{|k|} \right)^2 \frac{J_n^2\,(k_\perp v_\perp/\Omega_e)}{v^4\,|v_\parallel - \partial\omega_k/\partial k_\parallel|}, \quad (2)$$

$k_\perp$ and $k_{||}$ are the components of the wave vector perpendicular and parallel to the ambient magnetic field $\mathbf{B_o}$, respectively, $k_{res} = (\omega_k - n\Omega_e)/v_{||}$ is the resonant parallel wave number, $\Omega_e = |eB_o/m_e|$ is the (angular) electron gyrofrequency, ω_k is the wave frequency as a function of k, E_k is the wave electric field at each k, and α and v are the particle pitch-angle and velocity, respectively. V is plasma volume, e/m_e is the electron charge to mass ratio, and J_n is the Bessel function of order n. We express the wave electric field E_k in the form[16]

$$|E_k|^2 = [V/N(\omega)]\,E^2(\omega)\,g_\omega(\theta), \quad (3)$$

where

$$E^2(\omega) = E^2_{wave} \frac{f(\omega)}{\int f(\omega)\,d\omega} \quad (4)$$

and

$$g_\omega(\theta) = \exp\left[-\left(\frac{x - x_o}{x_\omega} \right)^2 \right]. \quad (5)$$

Here, $x = \cos\theta$, θ is the wave normal angle (the angle between $\mathbf{B_o}$ and $\mathbf{k}$), $x_o = \cos 89°$, $g_\omega(\theta)$ gives the variation of wave electric field energy with wave normal angle. The parameter x_ω determines the angular width of the wave electric field energy. It is set equal to 0.01. The function $f(\omega)$ determines the distribution of wave energy with wave frequency. It is obtained by solving the dispersion relation for electrostatic ECH waves,[13] and $N(\omega)$ is the normalization constant.

Solution of the hot plasma dispersion relation has been provided in an early work.[10] In this work, HOTRAY code[25] is used to solve the linear dispersion relation for electrostatic waves generated by loss-cone distribution and wave dispersion and temporal growth rates are obtained. It is found that the peak growth rate occurs for propagation at $\theta \approx 89°$ and decreases sharply with decreasing (and increasing) the angle

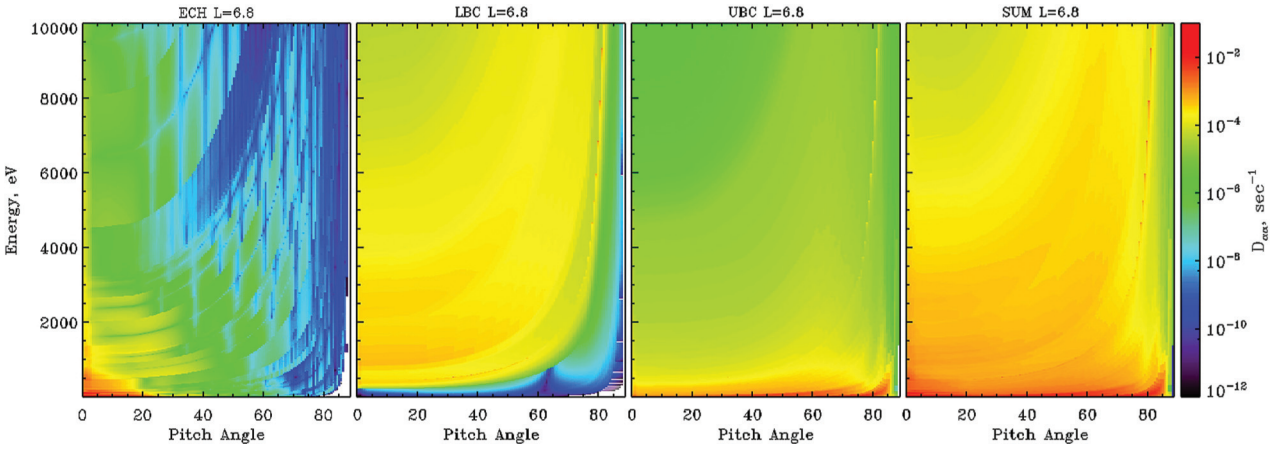

FIG. 2. Same as in Fig. 1 but for L = 6.8.

θ with an angular width $\Delta\theta = 0.5^\circ$. The values of parameters x_o and x_ω used in the present work are generally consistent with these calculations.

The momentum diffusion rate D_{pp} can be obtained by[9]

$$D_{pp} = D_{\alpha\alpha}\left[\frac{\sin\alpha\,\cos\alpha}{(n\Omega_e/\omega_k) - \sin^2\alpha}\right]^2. \tag{6}$$

Energy diffusion rate D_{EE} is related to D_{pp} by

$$D_{EE} = \left(\frac{E + 2E_o}{E + E_o}\right)^2 D_{pp}, \tag{7}$$

where E is the kinetic energy and E_o is the rest energy of the electron. For $E \ll E_o$, Eq. (7) is simply

$$D_{EE} = 4\,D_{pp}. \tag{8}$$

B. Whistler mode waves

Pitch-angle diffusion coefficients for whistler mode waves are given[16,26] in units of per second

$$D_{\alpha\alpha} = \sum_{n=-\infty}^{\infty} \int_0^{x_{max}} x\,dx\; D_{\alpha\alpha}^{nx}, \tag{9}$$

where $x = \tan\theta$ and $D_{\alpha\alpha}^{nx}$ is given by

$$D_{\alpha\alpha}^{nx} = \frac{\pi\,\cos^5\theta\,\Omega_e\left(-\sin^2\alpha - n\Omega_e/\omega_k\right)^2\,|\phi_{n,k}|^2}{2\,C_1\,\psi^{3/2}|1 + n\Omega_e/\omega_k|^3\,I(\omega_k)} \times f(\omega)\,g_\omega(x)\left(1 - \frac{1}{v_\parallel}\frac{\partial\omega_k}{\partial k_\parallel}|_x\right)^{-1}_{k_\parallel = k\,res} \times \left(\Omega_e\frac{B_{wave}^2}{B_o^2}\right), \tag{10}$$

where B_{wave} is wave magnetic field, $f(\omega)$ is the wave magnetic field spectral density, and $g_\omega(x)$ gives the wave normal distribution. $C_1 = \int f(\omega)d\omega$. $f(\omega)$ is obtained by solving the dispersion relation for whistler mode waves.[13] $g_\omega(x)$ is expressed as

$$g_w(x) = \exp[-(x/x_w)^2], \tag{11}$$

where x_ω is set equal to 1.0 since the wave normal distribution of chorus wave power is generally broad.[16,20] The expression for $|\phi_{n,k}|^2$ is given by

$$|\phi_{n,k}|^2 = \left[\left(\frac{D}{\mu^2 - S}\right)^2\left(\frac{\mu^2\sin^2\theta - P}{\mu^2}\right)^2 + \left(\frac{P\cos\theta}{\mu^2}\right)^2\right]^{-1} \times \left[\frac{\mu^2\sin^2\theta - P}{2\mu^2}\left(1 + \frac{D}{\mu^2 - S}\right)J_{n+1} + \frac{\mu^2\sin^2\theta - P}{2\mu^2}\left(1 - \frac{D}{\mu^2 - S}\right)J_{n-1} + J_n\cot\alpha\sin\theta\cos\theta\right]^2. \tag{12}$$

For a two-component plasma consisting of electrons and protons under the high density approximation ($(\omega_{pe}/\Omega_e)^2 \gg \omega/\Omega_e$, ω_{pe} is the electron plasma frequency), we write

$$\mu^2 = \frac{\omega_{pe}^2}{\Omega_e^2}\frac{1 + M}{M}\,\psi^{-1}, \quad M = m_e/m_p, \tag{13}$$

$$\psi = 1 - \frac{\omega_k^2}{\Omega_p\Omega_e} - \frac{\sin^2\theta}{2} + \left[\frac{\sin^4\theta}{4} + \left(\frac{\omega_k}{\Omega_p}\right)^2(1 - M)^2\cos^2\theta\right]^{1/2}, \tag{14}$$

where m_p is the mass of proton and Ω_p is the proton cyclotron frequency,

$$P = -\frac{\omega_{pe}^2}{\Omega_e^2}\frac{\Omega_e^2}{\omega_k^2}(1 + M), \tag{15}$$

$$S = 1/2\,(R + L),\; D = 1/2\,(R - L), \quad \text{and} \quad \left.\begin{matrix} R \\ L \end{matrix}\right\} = \pm\frac{\omega_{pe}^2}{\Omega_e^2}\frac{\Omega_e}{\omega_k}\left[\frac{1 + M}{1 - M \mp (\omega_k/\Omega_e - \Omega_p/\omega_k)}\right]. \tag{16}$$

Expressions for $I(\omega_k)$ and $\frac{\partial \omega_k}{\partial k_{||}}|_x$ are also obtained under the high density approximation. The expressions of momentum and energy diffusion coefficients are obtained using Eqs. (6)–(8).

During resonant wave-particle interactions, whistler mode can hit the Landau resonance if oblique propagation effects are included.[27,28] The wave could hit more than one resonance, that is, one resonance will amplify it (cyclotron) and the other (Landau) will damp it. In the limit of exactly parallel propagation (i.e., $\theta = 0$), there cannot be Landau resonance between electrons and whistler mode waves. Since wave propagation at an angle to the magnetic field is included in the present study, we calculate the diffusion rates for Landau ($n = 0$) and $\pm 1, \ldots, \pm 5$ cyclotron harmonic resonances.

III. RESONANT FREQUENCIES

A. ECH waves

Resonant frequencies for given electron energy, pitch angle, and wave normal angle can be obtained using the resonant condition and the dispersion relation for ECH waves. The resonance condition is

$$k_{||} = (\omega - n\,\Omega_e)/v_{||}, \quad n = 0, \pm 1, \ldots\ldots \pm 5\,. \tag{17}$$

The dispersion relation can be written as[29]

$$1 = \frac{2\,\omega_{pe}^2}{\lambda} \sum_{n=1}^{\infty} e^{-\lambda} I_n(\lambda)\, \frac{n^2}{\omega^2 - n^2\,\Omega_e^2} + \omega\,\omega_{pe}^2\, \cos^2\theta\, e^{-\lambda} \sum_{n=-\infty}^{+\infty} I_n(\lambda)\, \frac{1}{(\omega - n\,\Omega_e)^3}, \tag{18}$$

where $\lambda = T_c\, k_\perp^2 / m_e\, \Omega_e^2$ and $I_n(\lambda)$ are modified Bessel function. T_c is the cold electron temperature. For ECH waves, the wave power maximizes at $\theta = 89°$ (Eq. (5)). The wave normal angle (θ) is assumed to be 89°. Calculations of resonant frequencies have been carried out for cyclotron harmonics $n = +1$, $+2$, and $+3$.

B. Whistler mode waves

The dispersion relation for whistler mode waves for cold plasma[30] under the high density approximation is given as[16]

$$\frac{c^2 k^2}{\omega^2} = \frac{\omega_{pe}^2}{\Omega_e^2}\, \frac{1+M}{M}\, \psi^{-1}, \tag{19}$$

where $\psi = 1 - \frac{\omega^2}{\Omega_p \Omega_e} - \sin^2\theta/2 + [\sin^4\theta/4 + (\omega/\Omega_p)^2 (1-M)^2 \cos^2\theta]^{1/2}$.

For given electron energy, pitch angle, and wave normal angle, resonant frequencies can be obtained using the resonant condition (Eq. (17)) and dispersion relation (Eq. (19)). Calculations of resonant frequencies have been carried out for Landau resonance for a representative wave normal angle $\theta = 10°$.

IV. RESULTS AND DISCUSSION

In Figs. 1 and 2, we have presented pitch angle diffusion coefficients ($D_{\alpha\alpha}$) for different types of waves (ECH, LBC, UBC) at two spatial locations $L = 4.6$ and 6.8, respectively. These are shown as a color coded two dimensional image of the diffusion coefficients in the pitch-angle−energy space. A color table on the right corresponds to displayed values of the $D_{\alpha\alpha}$ in the range from 1.0×10^{-12} to $0.1\ s^{-1}$. However, all values below $1.0 \times 10^{-12}\ s^{-1}$ due to its insignificance are not displayed and therefore there are gaps. Calculations of diffusion coefficients are based on plasma parameters measured by PWE, LEPA, and fluxgate magnetometer onboard the Combined Release and Radiation Effects Satellite (CRRES).[13,31] These physical parameters are for $L = 4.6$: $n_c = 21.5\ cm^{-3}$, $T_c = 4\ eV$, $B_o = 312\ nT$ and for $L = 6.8$: $n_c = 12.0\ cm^{-3}$, $T_c = 10\ eV$, $B_o = 92.5\ nT$. The amplitude of magnetic field for LBC and UBC waves is taken to be 10 pT, and for ECH waves, a value of $1\ mVm^{-1}$ is used. These values are within the range of observed wave database from CRRES.[32] Further, we have used the calculated temporal growth rate profile[13] to represent the wave spectral density distribution in the calculation of diffusion coefficients for ECH and whistler mode waves. Landau resonance ($n = 0$) and cyclotron harmonic resonances $n = \pm 1, \ldots \pm 5$ have been included in the diffusion coefficients calculations.

In Fig. 1, it is noted that there are large dips, oscillations, and gaps in the profile of $D_{\alpha\alpha}$ versus PA at energies ≥ 1 keV for ECH and >2 keV for LBC waves. The structures can also be seen in profile of $D_{\alpha\alpha}$ as shown in Fig. 2, although here the structures are not so prominent. It may be noted from Eqs. (1) and (10) that the PA variation in diffusion coefficient appears due to two sources. First, there is an explicit dependence of diffusion coefficients on PA. Second, there is an implicit dependence of diffusion coefficients on PA through the resonant frequency $\bar{\omega}_r\ (= \omega_r/\Omega_e)$. Resonant frequency depends on PA as can be seen in Eq. (17). To complete the present study, we have also calculated momentum diffusion coefficients (D_{pp}) at selected energies.

In Fig. 3, we present $D_{\alpha\alpha}$ (a) and D_{pp} (b) for ECH waves at $L = 4.6$ for two electron energies 1 keV and 10 keV. Diffusion coefficients at 10 keV are quite small. The banded structures are seen at 1 keV in both $D_{\alpha\alpha}$ and D_{pp} coefficients. In Figs. 4–6, we provide diffusion coefficients at $L = 4.6$ for individual resonances $n = +1$, $+2$, and $+3$, respectively,

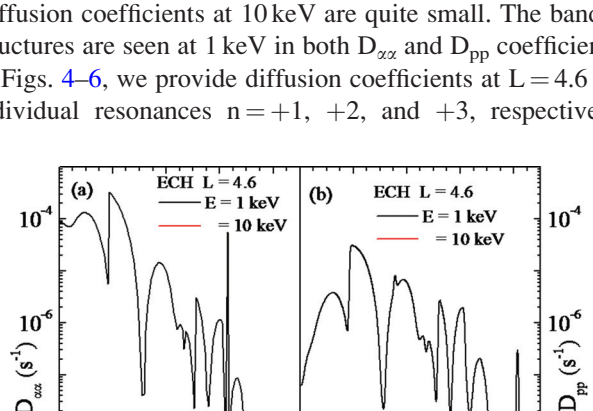

FIG. 3. Variation of pitch angle ($D_{\alpha\alpha}$) and momentum (D_{pp}) diffusion coefficients with pitch angle for ECH waves at $L = 4.6$ corresponding to electron energies 1 keV and 10 keV. (a) $D_{\alpha\alpha}$ and (b) D_{pp}.

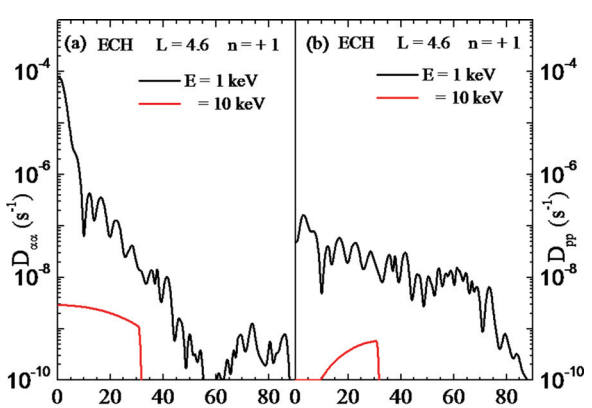

FIG. 4. Same as in Fig. 3 but for cyclotron resonance n = +1. (a) $D_{\alpha\alpha}$ and (b) D_{pp}.

having the same energies (i.e., 1 and 10 keV). It is found that $D_{\alpha\alpha}$ and D_{pp} at Landau (n = 0) resonance and other cyclotron resonances are in general quite small or even negligible. Further, the values of $D_{\alpha\alpha}$ and D_{pp} are not shown for 10 keV in Figs. 5 and 6 since these are found to be negligible or zero. It is seen that values of $D_{\alpha\alpha}$ for resonances n = +1 and +2 are comparable and one to two orders larger than values at n = +3. However, coefficient $D_{\alpha\alpha}$ at n = +1 covers a much smaller PA range as compared to that for resonance +2. The banded structures in the $D_{\alpha\alpha}$ profile are seen only in the case of n = +2 resonance (Fig. 5). Banded structures at +2 are also seen for energy 8 keV (not shown). The values of D_{pp} at resonance +1 are several orders of magnitude smaller than the values of $D_{\alpha\alpha}$ at the same resonance. However, the values of D_{pp} cover a much wider PA range as compared to those of $D_{\alpha\alpha}$ values. Values of D_{pp} for n = +2 are in general comparable to those of $D_{\alpha\alpha}$ and show the banded structures similar to those of $D_{\alpha\alpha}$ values. The values of D_{pp} for the case n = +3 are again several orders of magnitude smaller than those of $D_{\alpha\alpha}$ values. In Table I, we present the resonant frequencies of ECH waves for L = 4.6 for resonances n = +1, +2, and +3 by considering the wave normal angle 89°. It is noted that the resonant frequencies for n = +1 are in the region where the wave power is large. The temporal growth rate profile of ECH

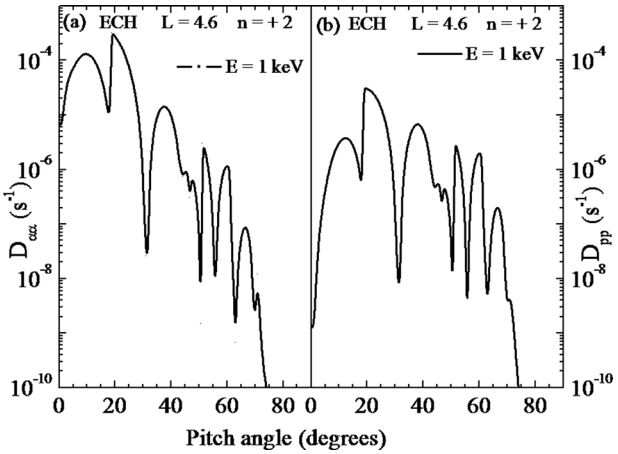

FIG. 5. Same as in Fig. 3 but for n = +2. Values at 10 keV are negligible and therefore not shown. (a) $D_{\alpha\alpha}$ and (b) D_{pp}.

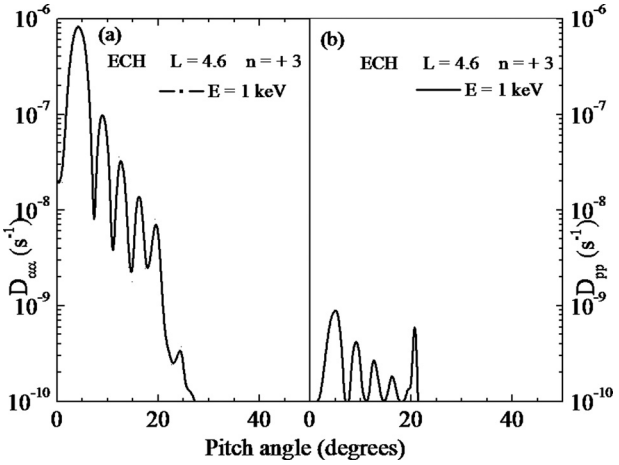

FIG. 6. Same as in Fig. 3 but for n = +3. Values at 10 keV are negligible and therefore not shown. (a) $D_{\alpha\alpha}$ and (b) D_{pp}.

waves at L = 4.6 is in the range of normalized frequencies[13] from 1.275 to 1.875.

Fig. 7 represents the variation of $D_{\alpha\alpha}$ and D_{pp} for ECH waves at L = 6.8 having energies 1 keV and 10 keV. It is observed that the banded structures are less prominent in this case. Figs. 8–10 describe the variation of $D_{\alpha\alpha}$ and D_{pp} profiles for resonances n = +1, +2, and +3, respectively, corresponding to the same L-shell and energies. It was found that other resonances provide very small contribution to $D_{\alpha\alpha}$ and D_{pp} profiles. The case n = +1 (Fig. 8) provides the maximum contribution to the $D_{\alpha\alpha}$ profile and covers a small PA range. The contributions of resonances n = +1 and +2 are comparable in the case of D_{pp} profiles. The contribution due to n = +3 to D_{pp} profiles is much smaller. For the case of n = +1, D_{pp} covers a much wider range of PA as compared to the PA range covered by $D_{\alpha\alpha}$ profiles. Further, the magnitudes of D_{pp} coefficients are found one to two orders smaller as compared to magnitudes of $D_{\alpha\alpha}$ coefficients. The banded structures are seen for n = +2 (Fig. 9) both for $D_{\alpha\alpha}$ and D_{pp} coefficients. In Table II, we present the resonant frequencies of ECH waves at L = 6.8 for resonances n = +1, +2, and +3 at the energies 1 keV and 10 keV. It is noted that for n = +1, resonant frequencies cover a wide PA range and exist in the region where wave power is large. The temporal growth rate profile of ECH waves at L-shell 6.8 covers the frequency range 1.225 to 1.825.

In Figs. 11 and 12, we present the variation of $D_{\alpha\alpha}$ and D_{pp} for LBC and UBC, respectively, corresponding to

TABLE I. Resonant frequencies ($\bar{\omega}_r$) of ECH waves for L = 4.6 at various PAs by considering three cyclotron harmonic resonances (n = +1, +2, and +3) and wave normal angle 89° at two electron energies.

E	n \ PA	0°	10°	20°	30°	40°	50°	60°	70°	80°	85°
1 keV	+1	1.48	1.42	1.42	1.42	1.38	1.38	1.33	1.23	1.17	1.12
	+2	1.23	1.23	1.17	1.17	1.12	1.12	1.08	1.08	1.08	…
	+3	1.08	1.08	1.08	1.08	1.08	1.08	1.08	1.08	…	…
10 keV	+1	1.77	1.77	1.73	1.73	1.67	1.62	1.58	1.48	1.33	1.23
	+2	1.97	1.97	1.97	1.97	1.97	1.97	…	1.27	1.08	1.08
	+3	1.38	1.38	1.33	1.27	1.23	1.17	1.12	1.08	1.08	1.08

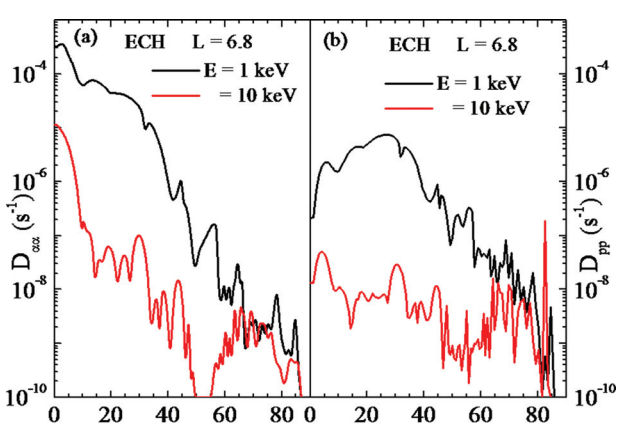

FIG. 7. Variation of pitch angle ($D_{\alpha\alpha}$) and momentum (D_{pp}) diffusion coefficients with pitch angle for ECH waves at L = 6.8 corresponding to electron energies 1 keV and 10 keV. (a) $D_{\alpha\alpha}$ and (b) D_{pp}.

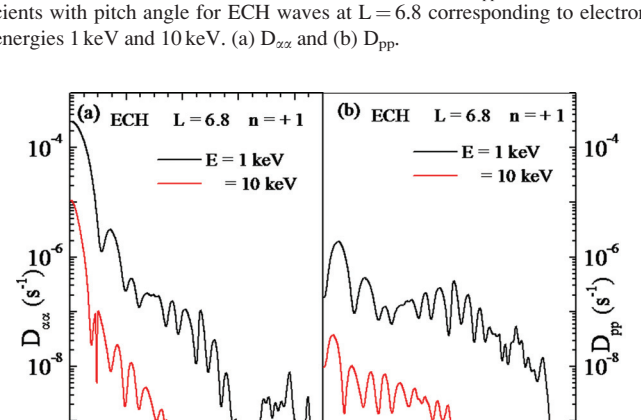

FIG. 8. Same as in Fig. 7 but for n = +1. (a) $D_{\alpha\alpha}$ and (b) D_{pp}.

L = 4.6. Calculations have been performed for two energies 3 keV and 10 keV by considering Landau (n = 0) resonance and all other cyclotron harmonic ($n \neq 0$) resonances. It may be noted that Landau resonance shows dips and banded structures in the $D_{\alpha\alpha}$ and D_{pp} profiles for LBC at both energies (Fig. 11), whereas the case ($n \neq 0$) shows a smooth behaviour. In UBC, the structures are seen in the Landau

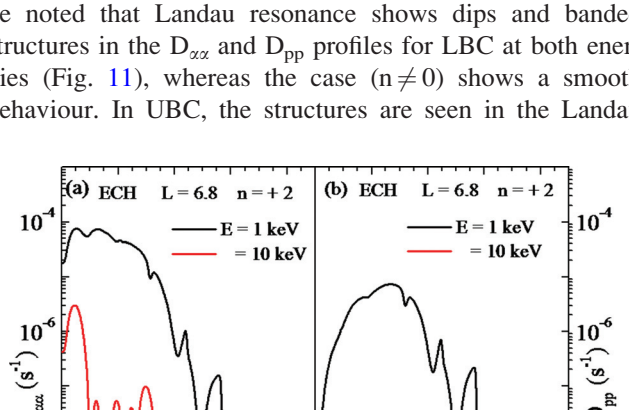

FIG. 9. Same as in Fig. 7 but for n = +2. (a) $D_{\alpha\alpha}$ and (b) D_{pp}.

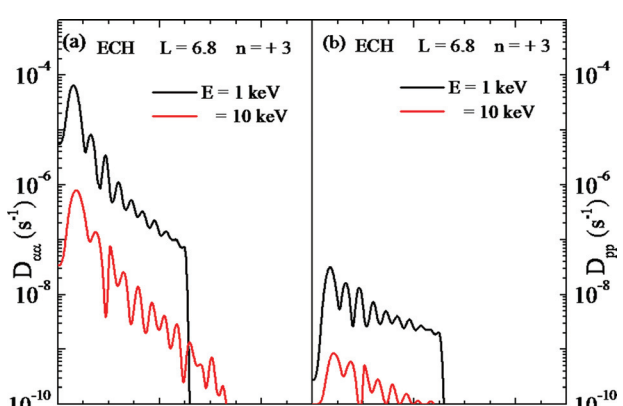

FIG. 10. Same as in Fig. 7 but for n = +3. (a) $D_{\alpha\alpha}$ and (b) D_{pp}.

TABLE II. Same as in Table I but for L = 6.8

E	PA / n	0°	10°	20°	30°	40°	50°	60°	70°	80°	85°
1 keV	+1	1.38	1.38	1.38	1.33	1.33	1.27	1.23	1.23	1.12	1.12
	+2	1.12	1.12	1.12	1.12	1.12	1.12	1.12	1.12	1.08	1.08
	+3	1.12	1.12	1.12	1.12	1.12	1.12	1.12	1.08	1.08	1.08
10 keV	+1	1.67	1.62	1.62	1.58	1.58	1.52	1.48	1.38	1.27	1.17
	+2	1.97	1.97	1.97	1.97	…	…	1.27	1.17	1.12	1.12
	+3	1.23	1.23	1.17	1.17	1.17	1.12	1.12	1.12	1.12	1.08

resonance for 10 keV only (Fig. 12). Further, the magnitude of D_{pp} for 10 keV is one to two orders lower than the $D_{\alpha\alpha}$ values. However, the magnitude of D_{pp} at 3 keV for Landau resonance is higher than the values of $D_{\alpha\alpha}$. Table III provides the resonant frequencies at L = 4.6 for whistler mode waves by considering Landau resonance having the wave normal angle of 10°. It is observed from Table III that the resonant frequencies for 10 keV are shifted to a range of higher pitch angles ≥60° as compared to the values of 3 keV. This is consistent with the profiles of n = 0 shown in Figs. 11 and 12.

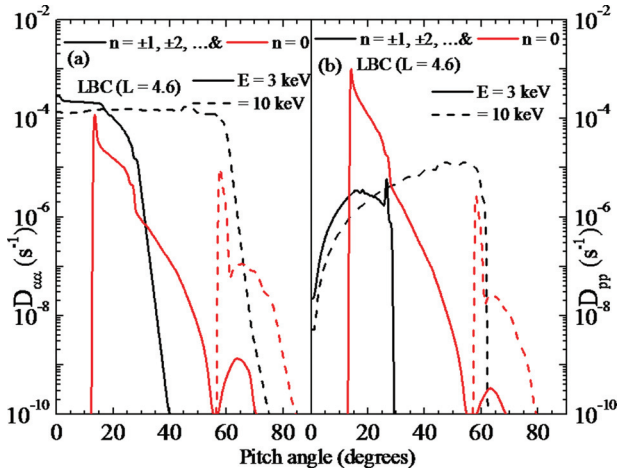

FIG. 11. Pitch angle ($D_{\alpha\alpha}$) and momentum (D_{pp}) diffusion coefficients of whistler mode (LBC) waves versus pitch angle for L = 4.6 at two energies 3 keV (solid line) and 10 keV (dashed line). Profiles are shown for Landau (n = 0) and ($n \neq 0$) resonances. (a) $D_{\alpha\alpha}$ and (b) D_{pp}.

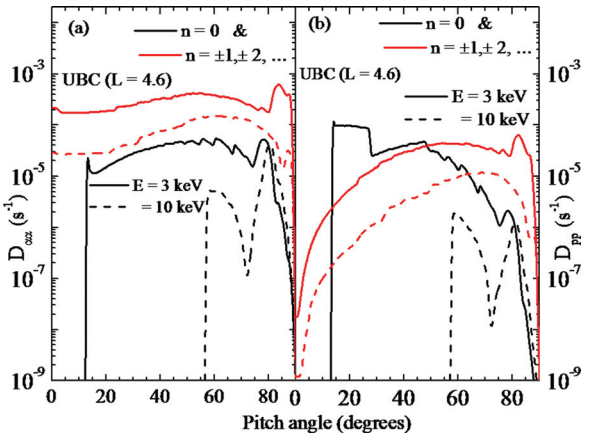

FIG. 12. Same as in Fig. 11 but for UBC waves. (a) $D_{\alpha\alpha}$ and (b) D_{pp}.

TABLE III. Resonant frequencies ($\bar{\omega}_r$) of whistler mode waves for L = 4.6 at various PAs by considering Landau (n = 0) resonance and wave normal angle 10° at three electron energies.

E \ PA	0°	10°	20°	30°	40°	50°	60°	70°	80°	85°
2 keV	0.23	0.22	0.19	0.16	0.12	0.08	0.05	0.02	0.005	0.0008
	07.6	0.77	0.79	0.83	0.87	0.91	0.94	0.96	0.98	0.98
3 keV	…	…	0.37	0.27	0.19	0.12	0.07	0.03	0.007	0.002
	…	…	0.61	0.71	0.79	0.86	0.91	0.95	0.98	0.98
10 keV	…	…	…	…	…	…	0.33	0.12	0.03	0.006
	…	…	…	…	…	…	0.66	0.87	0.96	0.98

Finally in Figs. 13 and 14, we present the $D_{\alpha\alpha}$ and D_{pp} profiles for LBC and UBC waves, respectively, at L = 6.8. Like L = 4.6, the calculations have been performed for Landau (n = 0) and other cyclotron harmonic resonances ($n \neq 0$) but for electron energies 500 eV and 1 keV. The reason for choosing lower energies as compared to the L = 4.6 profile is as follows. Resonant energy of the whistler mode wave is controlled by the magnetic energy per particle $E_M = (B_o^2/8\pi n_c)$. The values of E_M are 1.8 keV and 11 keV for L = 6.8 and

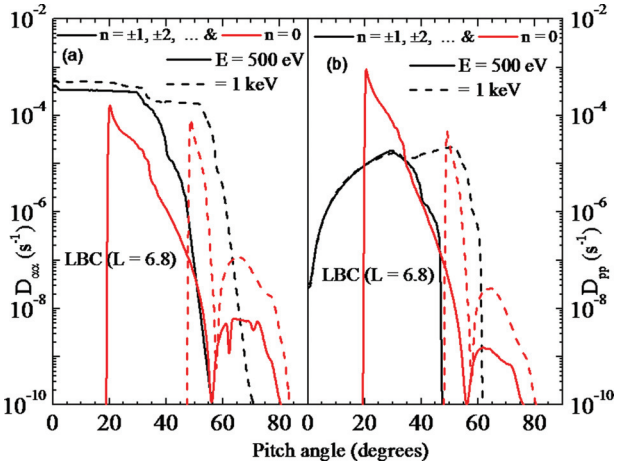

FIG. 13. Pitch angle ($D_{\alpha\alpha}$) and momentum (D_{pp}) diffusion coefficients of whistler mode (LBC) waves versus pitch angle for L = 6.8 at two energies 500 eV (solid line) and 1 keV (dashed line). Profiles are shown for both Landau (n = 0) and ($n \neq 0$) resonances. (a) $D_{\alpha\alpha}$ and (b) D_{pp}.

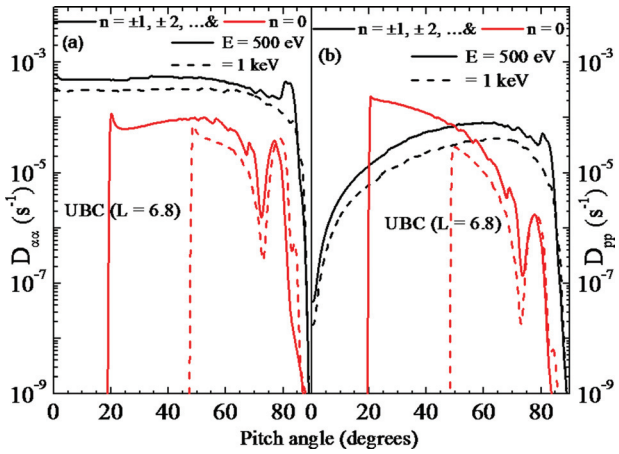

FIG. 14. Same as in Fig. 13 but for UBC waves. (a) $D_{\alpha\alpha}$ and (b) D_{pp}.

L = 4.6, respectively. It may be noted from Figs. 13 and 14 that dips and banded structures in $D_{\alpha\alpha}$ and D_{pp} profiles occur only for Landau resonance. Further, the banded structure in Landau resonance shifts to higher pitch angle ≥50° for energy 1 keV in comparison to the case of energy 500 eV. This behaviour is consistent with resonant frequencies for L = 6.8 presented in Table IV. From this table, it may also be noted that resonant frequencies for energy 10 keV shift to still higher PA ≥ 80° and fall outside the range of LBC and UBC frequencies.

Pitch angle and energy diffusion by whistler mode waves have previously been studied[23] for electron energies ≥30 keV using the CRRES data. The very narrow peaks in the diffusion rates are found near 80°, which correspond to diffusion by individual resonances, particularly the Landau (n = 0) and n = ±1 resonances. The high-order resonances occur at smaller pitch angles and add in such a way as to give a smoother profile. In the present study for electron energies ≤10 keV, we find almost similar results. However, in this study, narrow peaks in $D_{\alpha\alpha}$ and D_{pp} profiles are obtained due to Landau (n = 0) resonance, whereas the case $n \neq 0$ produces smooth profiles (Figs. 11 and 13).

V. CONCLUSIONS

In the present study, we have calculated electron pitch angle ($D_{\alpha\alpha}$) and momentum (D_{pp}) diffusion coefficients due to resonant interactions with ECH and whistler mode chorus

TABLE IV. Same as in Table III but for L = 6.8 and electron energies 200 eV, 500 eV, 1 keV, and 10 keV.

E \ PA	0°	10°	20°	30°	40°	50°	60°	70°	80°	85°
200 eV	0.13	0.12	0.11	0.09	0.07	0.05	0.03	0.01	0.003	0.0003
	0.86	0.86	0.87	0.89	0.91	0.94	0.96	0.97	0.98	0.98
500 eV	…	…	0.45	0.30	0.20	0.13	0.07	0.03	0.008	0.002
	…	…	0.53	0.69	0.78	0.85	0.91	0.95	0.98	0.98
1 keV	…	…	…	…	…	0.36	0.17	0.07	0.02	0.004
	…	…	…	…	…	0.62	0.82	0.91	0.97	0.98
10 keV	…	…	…	…	…	…	…	…	0.21	0.04
	…	…	…	…	…	…	…	…	0.77	0.94

waves. Calculations have been performed at two spatial locations $L = 4.6$ and $L = 6.8$ corresponding to electron energies ≤ 10 keV. In the calculation, Landau resonance ($n = 0$) and cyclotron harmonic resonances $n = \pm 1, \ldots \pm 5$ have been included. Calculations have also been performed for individual resonances. Resonant frequencies are calculated for ECH waves by considering the resonances $n = +1$, $+2$, $+3$ and wave normal angle $\sim 89°$. In case of whistler mode waves, resonant frequencies are calculated for Landau ($n = 0$) resonance at wave normal angle 10°. The main conclusion of studies are summarized as follows:

(1) Large dips, oscillations, and gaps or banded structures are seen in profiles of diffusion coefficients versus pitch angle. These structures are more pronounced in diffusion coefficients profiles for ECH and LBC waves particularly at $L = 4.6$.
(2) In case of ECH waves, the major contribution to $D_{\alpha\alpha}$ coefficients appears from harmonic resonances $n = +1$ and $+2$, whereas in D_{pp} coefficients appears from $+2$. However, banded structures in $D_{\alpha\alpha}$ and D_{pp} coefficients appear only for $n = +2$. For Landau and other harmonic resonances, values of diffusion coefficients are in general quite small or even negligible.
(3) For whistler mode chorus waves, the profiles of diffusion coefficients are quite smooth for all harmonic resonances included ($n \neq 0$). Banded structures appear only in the profiles of diffusion coefficients for Landau ($n = 0$) resonance.
(4) Diffusion coefficients profiles are in general consistent with the calculated resonant frequencies.
(5) In ECH waves, the banded structures appear mainly for electron energies ≥ 1 keV. But for LBC and UBC waves, the structures appear for energies >2 keV for $L = 4.6$ and >200 eV for $L = 6.8$.
(6) For ECH waves, the values of D_{pp} coefficients are one to two orders of magnitude smaller as compared to values of $D_{\alpha\alpha}$ coefficients. For LBC and UBC waves, D_{pp} coefficients is again in general an order of magnitude smaller than $D_{\alpha\alpha}$ coefficients but only for the case $n \neq 0$. For Landau resonance, the values of D_{pp} coefficients are generally larger than the values of $D_{\alpha\alpha}$ coefficients at energies 3 keV in case of $L = 4.6$ and 500 eV at 6.8.
(7) The "structures" have important implications for the effect of waves on electrons. The whistler mode can hit the Landau resonance for oblique propagation. The wave could hit more than one resonance,[28] that is, one resonance will amplify it (cyclotron) and the other (Landau) will damp it. This would, however, require two electron components: a warm component with a small thermal spread (background electrons) and a less dense hotter component. The background electrons provide the damping and the hot electrons (represented by a bi-Maxwellian distribution function) provide the drive. We have found the orders of resonance that make the main contributions to $D_{\alpha\alpha}$ and D_{pp} coefficients.

Further, the present work will be helpful in the study of diffusion curves, which are the paths followed by the electrons as they diffuse through the velocity space. Many diffusion curves are possible for the interaction with ECH waves depending on the order of resonance. We find that the cyclotron resonances $n = +1$ and $+2$ give the main contribution to diffusion coefficients. For obliquely propagating whistler mode waves, the Landau resonance produces the structures.

(8) These results will have important consequences for diffuse aurora and pancake distributions. Highly anisotropic electron velocity distributions, peaked near 90° to the magnetic field, are called pancakes from their appearance in velocity space. The distributions have been characterized by a pancake index, which is the flux ratio between 90° and 70°. It has been suggested[31] that whistler mode waves play a dominant role in the production of diffuse aurora and in the formation of pancake distributions outside $L = 6.0$, whereas inside $L = 6.0$, ECH waves also play a significant role. Pancakes should form as a result of wave-particle interaction if the particle diffusion becomes weaker at a large pitch angle close to 90°. Diffuse aurora is controlled[33] by the diffusion coefficient $D_{\alpha\alpha}$ at the edge of the loss-cone. We find that the ECH waves would contribute in the production of diffuse aurora at cyclotron resonances $n = +1$ and $+2$.

It may also be noted that at 1 keV, coefficient $D_{\alpha\alpha}$ for cyclotron resonance $n = +1$ extends to pitch angles up to about 40°. For $n = +2$, coefficient $D_{\alpha\alpha}$ for ECH waves extends to larger pitch angles, about 60°–70° at $L = 4.6$ and 50°–60° at $L = 6.8$.

Therefore, both resonances would contribute to the formation of pancake distributions.

The banded structures should be reflected in the pancake distributions. The effect of banded structures is more pronounced at $L = 4.6$ as compared to $L = 6.8$.

The whistler mode waves would contribute to the production of diffuse aurora for all cyclotron resonances ($n \neq 0$). Further, for LBC waves, all resonances (including Landau resonance) would contribute to the formation of pancakes. However, UBC waves would not contribute to the formation of pancakes since coefficient $D_{\alpha\alpha}$ for UBC extends close to pitch angle 90°. The coefficient $D_{\alpha\alpha}$ for LBC waves extends to lower pitch angles of about 70°. As for ECH waves, the banded structures should be reflected in the pancake distributions from LBC waves.

ACKNOWLEDGMENTS

This work was supported with financial assistance provided by the Planetary Sciences and Exploration Programme, Indian Space Research Organization (ISRO), PRL, Ahmedabad, under the sanctioned PLANEX project scheme. Funding support for this study was also provided by NASA Van Allen Probes (formerly known as the Radiation Belt Storm Probes (RBSP)) Project, the NASA LWS Program, and by the Indian Institute of Technology (Banaras Hindu University), India. The data for this paper are available from George V. Khazanov at george.v.khazanov@nasa.gov. Calculations reported in the present work were carried out at the Computer Centre, Banaras Hindu University.

[1]B. Ni, R. M. Thorne, Y. Y. Shprits, and J. Bortnik, Geophys. Res. Lett. **35**, L11106, doi:10.1029/2008GL034032 (2008).
[2]B. T. Tsurutani and E. J. Smith, J. Geophys. Res. **79**, 118, doi:10.1029/JA079i001p00118 (1974).
[3]W. J. Burtis and R. A. Helliwell, Planet. Space Sci. **24**, 1007 (1976).
[4]N. P. Meredith, R. B. Horne, and R. R. Anderson, J. Geophys. Res. **106**, 13165, doi:10.1029/2000JA900156 (2001).
[5]W. Li, R. M. Thorne, V. Angelopoulas, J. Bortnik, C. M. Cully, B. Ni, O. Le Contel, A. Roux, U. Auster, and W. Magnes, Geophys. Res. Lett. **36**, L09104, doi:10.1029/2009GL037595 (2009).
[6]M. Hayakawa, Y. Yamanaka, M. Perrot, and F. Lefeuvre, J. Geophys. Res. **89**, 2811, doi:10.1029/JA089iA05p02811 (1984).
[7]N. Haque, M. Spasojevic, O. Santolik, and U. S. Inan, J. Geophys. Res. **115**, A00F07, doi:10.1029/2009JA014717 (2010).
[8]D. A. Gurnett and A. Bhattacharjee, *Instruction to Plasma Physics: With Space and Laboratory Applications* (Cambridge University Press, Cambridge, United Kingdom, 2005).
[9]L. R. Lyons, J. Geophys. Res. **79**, 575, doi:10.1029/JA079i004p00575 (1974).
[10]R. B. Horne and R. M. Thorne, J. Geophys. Res. **105**, 5391, doi:10.1029/1999JA900447 (2000).
[11]A. K. Tripathi and R. P. Singhal, Phys. Plasmas **16**, 112107 (2009).
[12]B. Ni, R. M. Thorne, R. B. Horne, N. P. Meredith, Y. Y. Shprits, L. Chen, and W. Li, J. Geophys. Res. **116**, A04218, doi:10.1029/2010JA016232 (2011).
[13]A. K. Tripathi, R. P. Singhal, K. P. Singh, and O. N. Singh II, J. Atmos. Sol.–Terr. Phys. **97**, 125 (2013).
[14]X.-J. Zhang, V. Angelopoulos, B. Ni, and R. M. Thorne, J. Geophys. Res. **120**, 292, doi:10.1002/2014JA020455 (2015).
[15]G. V. Khazanov, A. K. Tripathi, R. P. Singhal, E. W. Himwich, A. Glocer, and D. G. Sibeck, J. Geophys. Res. **120**, 445, doi:10.1002/2014JA020641 (2015).
[16]L. R. Lyons, J. Plasma Phys. **12**, 417 (1974).
[17]R. M. Thorne, B. Ni, X. Tao, R. B. Horne, and N. P. Meredith, Nature **467**, 943 (2010).
[18]Z. Su, H. Zheng, and S. Wang, J. Geophys. Res. **114**, A08202, doi:10.1029/2009JA014269 (2009).
[19]Z. Su, H. Zheng, and S. Wang, J. Geophys. Res. **115**, A05219, doi:10.1029/2009JA014759 (2010).
[20]B. Ni, R. M. Thorne, N. P. Meredith, R. B. Horne, and Y. Y. Shprits, J. Geophys. Res. **116**, A04219, doi:10.1029/2010JA016233 (2011).
[21]G. V. Khazanov, A. K. Tripathi, D. G. Sibeck, E. W. Himwich, A. Glocer, and R. P. Singhal, J. Geophys. Res. **120**, 9891, doi:10.1002/2015JA021728 (2015).
[22]R. B. Horne and R. M. Thorne, Geophys. Res. Lett. **30**, 1527, doi:10.1029/2003GL016973 (2003).
[23]R. B. Horne, R. M. Thorne, S. A. Glauart, J. M. Albert, N. P. Meredith, and R. R. Anderson, J. Geophys. Res. **110**, A03225, doi:10.1029/2004JA010811 (2005).
[24]D. Summers, B. Ni, and N. P. Meredith, J. Geophys. Res. **112**, A04207, doi:10.1029/2006JA011993 (2007).
[25]R. B. Horne, J. Geophys. Res. **94**, 8895, doi:10.1029/JA094iA07p08895 (1989).
[26]R. P. Singhal and A. K. Tripathi, Ann. Geophys. **24**, 1705 (2006).
[27]R. B. Horne, S. A. Glauart, and R. M. Thorne, Geophys. Res. Lett. **30**, 1493, doi:10.1029/2003GL016963 (2003).
[28]A. R. Soto-Chavez, G. Wang, A. Bhattacharjee, G. Y. Fu, and H. M. Smith, Geophys. Res. Lett. **41**, 1838, doi:10.1002/2014GL059320 (2014).
[29]A. K. Tripathi and R. P. Singhal, J. Geophys. Res. **110**, A12205, doi:10.1029/2005JA011113 (2005).
[30]T. H. Stix, *The Theory of Plasma Waves* (McGraw-Hill, 1962).
[31]N. P. Meredith, A. D. Johnstone, S. Szita, R. B. Horne, and R. R. Anderson, J. Geophys. Res. **104**, 12431, doi:10.1029/1998JA900083 (1999).
[32]N. P. Meredith, R. B. Horne, R. M. Thorne, and R. R. Anderson, J. Geophys. Res. **114**, A07218, doi:10.1029/2009JA014230 (2009).
[33]Y. Y. Shprits, W. Li, and R. M. Thorne, J. Geophys. Res. **111**, A12206, doi:10.1029/2006JA011758 (2006).